Editors' Suggestion

Interplay between Geometry, Fluid Dynamics, and Structure in the Ventricles of the Human Heart

Dario Collia,[1] Giulia Pedrizzetti,[2] Tomoyuki Sato,[3] Daisuke Matsubara,[3] Luigino Zovatto,[1] Massimiliano Gei,[1] Anirban Banerjee,[3] and Gianni Pedrizzetti[1,4,*]

[1] *Department of Engineering and Architecture, University of Trieste, Trieste 34127, Italy*

[2] *Department of Chemical Engineering, Materials, Environment, University of Roma "La Sapienza", Rome 00185, Italy*

[3] *Department of Pediatrics, Division of Cardiology, The Children's Hospital of Philadelphia, University of Pennsylvania, Pennsylvania 19104, USA*

[4] *Department of Biomedical Engineering, University of California, Irvine, California, USA*

(Received 9 September 2022; revised 31 October 2022; accepted 7 November 2022; published 4 January 2023)

Natural structures conveying fluid flow exhibit an interplay between flow-mediated forces and long-term adaptation. This phenomenon is relevant in the cardiovascular system where the geometric remodeling of the heart chambers is the main mechanism underlying pathological progression leading to hearth failure. Cardiac adaptation is analyzed here in children with a single right ventricle (SRV) in their heart. In these patients, the left ventricle (LV) is not well developed and the healthy right ventricle (RV) is surgically reconnected, early after birth, to take the functional role of the systemic ventricle. Such a condition represents a special model to investigate cardiac adaptation and this study takes advantage of the availability of an uncommon dataset (64 normal RVs, 64 normal LVs, 64 SRVs with clinically normal function). The ventricular functional performance is analyzed in terms of fluid dynamics and tissue deformation with the objective of verifying to which degree the SRV configuration adapts from the original RV and progresses toward the function of a LV. Results show that the SRV immediately assumes a larger volume and a wider geometry due to the higher operating pressure. However, the fluid dynamics is weakly turbulent and produces a reduced propulsion. The surrounding tissue develops muscular thickening with multidirectional orientation of myofibers that mimic a LV. However, the reduced flow performance and a lower structural consistency makes the SRV at higher risk of progressive dysfunctional adaptations. This study demonstrates how the interplay between cardiac flow and tissue response represents the driving macroscopic factor underlying the development of heart failure. More in general, the combined evaluation of fluid dynamics and structural functional properties can be a requirement for the exploration of adaptation processes across the different time scales.

DOI: 10.1103/PhysRevApplied.19.014006

I. INTRODUCTION

The dynamic interplay between flowing fluids and surrounding solid elements represents a foundation of long-term reciprocal adaptive behaviors in numerous disciplines, from environmental, climate studies to industrial applications, to physiological systems. Flowing water and prevailing winds in the lower atmosphere interact with the landscape and design its long-term shape. Rivers find the best path to cross a land and modify it through an interactive optimization between flow and terrain. During this process, the riverbed creates bedforms out of sand, like dunes and ripples, that influence the flow energetic balance, which in turn modifies how the flow interacts with the surrounding terrain [1]. The concept of structures designed by the flow is also entering the field of industrial applications, where engineers have started developing novel design techniques to reproduce solutions inspired by nature and biology. To this end, computational fluid dynamics is used to optimize the shape of elements in relation to their desired function, namely by starting from a rough design and reproducing its expected long-term evolution that is optimal in relation to its function [2] (an approach sometimes included in the category of biomimicry or bionics).

As a general concept, the adaptation of a structure delegated to perform a fluid dynamics function inevitably affects the function itself; vice versa, a modification of the functional requirement may induce progressive geometrical changes in an adaptive structure. This interplay

*giannip@dia.units.it

about geometry and function is often not evident, hidden by the longer time scale required for structural changes with respect to the rapid response of flowing fluids.

The interplay between fluid flow and surrounding boundaries is particularly active in biological systems. Here the surrounding tissues are able to progressively adapt, following the stimulation given by the moving fluid that is often responsible for shaping biological structures. An example of paramount relevance is the function of the mammalian heart: it is central for life, beating about 10^5 times every day and suiting largely varying conditions, from birth to oldness through extreme sport or pathologies.

Blood motion in the human heart represents a vigorous dynamic phenomenon: blood enters with velocities about 1 ms^{-1} into a cavity a few centimeters long and, within a few tenths of a second, it has to rotate nearly 180° and exit at a similar speed. This phenomenon involves an intense exchange of momentum between blood and the nearby cardiac tissues. Recent experimental studies demonstrated how small alterations of cardiac flow during the early embryonic stages severely modifies the geometry of the growing heart [3–5]. At the same time, clinical studies in children and adults brought initial evidences about the potential role of flow-driven forces to modulate cardiac adaptation in the presence of a pathology or during a healing process [6–9]. The progressive transformation of cardiac geometry due to pathological adaptation is known as cardiac adverse remodeling, which also alters the cardiac function and can lead to heart failure. Vice versa, previously diseased hearts undergo through reverse remodeling during healing.

Cardiac remodeling represents one prototypical interplay between living tissue and fluid motion; at the same time, its improved understanding is of paramount relevance in clinical cardiology. The relationship between geometry, fluid dynamic function, and structural adaptation is here analyzed in the case of children with a single right ventricle (SRV). The condition of a SRV is found in children that present at birth with a condition known as hypoplastic left heart syndrome [10]. These patients have, structurally, a normal right ventricle (RV) and a largely underdeveloped left ventricle (LV). They undergo a series of surgical procedures to ensure survival during the first several months of life that culminates, between 2 to 4 years of age, with a procedure (Fontan procedure) where the right heart is bypassed (caval veins are directly connected to the pulmonary arteries). After the Fontan procedure, the RV mainly receives oxygenated blood and serves as the systemic ventricle in the absence of a useful LV. Unfortunately, the survival rate of these patients remains low in the long term [11,12] indicating that adaptation is often inadequate.

Therefore, the SRV represents an interesting model to investigate *in vivo* long-term adaptive response in the heart chambers because the SRV is required to change its function from that of a RV, originally structured for supporting the pulmonary circulation only, to the more demanding effort required by a LV supporting the systemic circulation. This functional modification is expected to push the original RV to eventually behave similarly to a LV. Such modifications were analyzed in terms of volumes and global properties in relation to clinical outcome [13,14]. The common assumption is that the SRV function lies somewhere in between the LV and RV; however, detailed mechanistic analyses are not available, as well as conceptual models that make it possible to discriminate those situations where ventricular function allows a normal life from those where the SRV adaptation progresses toward heart failure.

The present study describes how the novel functional requirement for the SRV develops within the original RV structure. The analysis is performed by a combined mechanical analysis that involves both intracavitary fluid dynamics, to describe changes in pumping function, and tissue deformation, to identify the longer-term adaptations in the tissue. To this end, a comparative analysis of normal RVs, normal LVs, and clinically matched SRVs is carried out, exploiting availability of a valuable *in vivo* dataset. This study aims to present a physics-based background for the analysis of mechanical function that can be a reference for future systematic clinical studies. While clinical considerations are beyond the scope of this work, it applies a physics-based approach with the objective to learn more about the interplay between functional requirements and structural adaptations.

II. DATA

A. Clinical data

The analysis included a group of 64 patients with a SRV with a clinically normal and stable function and homogeneous characteristics, excluding pathology variants (e.g., atrioventricular canal, double outlet RV, septal defects, critical aortic stenosis, severe tricuspid regurgitation) [15]. The presence of pathological variants would have an impact on SRV function; this aspect is not addressed by design to keep the study simple. To this end, it also included a group of 64 RVs and a third group of 64 LVs in age-matched subjects without any identified cardiac disease and normal function. Age ranged approximately between 2 and 18 years old with a gender division of 40% female to 60% male; the ensemble median age at echocardiography was 10.6 yr (first and third quartiles 6.3–15.3) with no statistical difference between groups. For reference, the age of Fontan in the SRV groups was 2.8 (quartiles 2.1–3.2) and the duration between Fontan and echocardiography was 7.3 (quartiles 3.7–12.2). Heart rate (77 beats per minute on average) and blood pressure in the systemic circulation (108 and 61 mmHg in systole and diastole, respectively) were also statistically comparable in

the three groups. Children in the SRV group were slightly smaller (average body surface area, BSA = 1.02 m^2) than the others (1.36 m^2). The study was approved by the Institutional Review Board of The Children's Hospital of Philadelphia and all participants or their guardians provided informed consent to the usage of data in anonymous form for research.

All 192 subjects underwent three-dimensional (3D) echocardiography as per institutional clinical practice; recordings were spatially focused on the ventricle under analysis and presented an average time resolution of 32 Hz (corresponding to about 25 frames per heartbeat). The 3D imaging datasets were initially analyzed by dedicated software (4D RV Function and 4D LV Analysis, TomTec Imaging System GmbH, Unterschleissheim, Germany) to extract the ventricular geometry. The boundary (endocardium) between the ventricular tissue and blood pool is first drawn manually through the graphical user interface at one instant, then the software tracks the anatomical features over the entire heartbeat by optical flow methods. This analysis produces a triangulated surface of the moving geometry where vertices identify material points.

B. Geometry

The geometries of the RV, LV, and SRV, properly averaged over each group, are reported in Fig. 1. To perform such an averaging procedure, all ventricles in a set are translated to a common center, then the anatomical landmarks (position of the two valves and apex) are identified and a 3D rotation is performed to bring all ventricles to a common axis (the direction from the midpoint between the valves' center to the apex) and aligned valvular position. The RV presents a slender and thin chamber, as it wraps around the LV that is more compact and with nearly circular cross sections; the SRV geometry is more rounded than the original RV and becomes more similar to that of the LV. This shape modification is a known physiological adaptation due to the higher systemic pressure loading either the SRV or LV (on average close to 100 mmHg), with respect to that in the pulmonary circulation (about 10 mmHg) acting on the right side. Because of the need to support a higher load, the normal LV muscular tissue is also much thicker than the RV. Such a pressure increase is considered the main factor that modifies the SRV geometry with respect to the RV, making it more rounded and building up the thickness of the muscular tissue. It also inflates the SRV to higher volumes than the normal RV, which in turn are physiologically slightly larger than the LV as well. The range from maximum to minimum values (from end diastole to end systole) is 90–39 cm^3 (RV), 82–31 cm^3 (LV), and 111–57 cm^3 (SRV).

In summary, the geometrical adaptation of an original RV into a SRV appears to drive it toward a shape that is more similar to the LV. However, this change develops over a RV anatomical structure that differs substantially from the LV; therefore, the resulting SRV may differ from both the RV and LV in terms of the fluid dynamics pumping function and tissue contraction pattern.

III. FLUID DYNAMICS

A. Methods and theory

The heart's function is about creating and sustaining blood motion. This is achieved through a contraction-relaxation sequence in the myocardial muscle; however, the ultimate aim is that of creating blood flow. Thus, any muscular activity is efficient when it is associated with high propulsion of blood toward the outflow (during ventricular

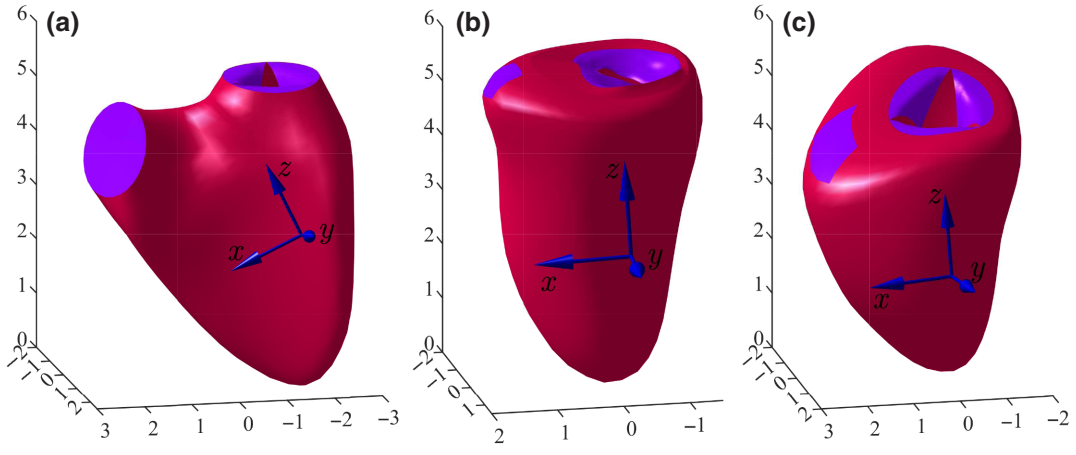

FIG. 1. Population-average geometry, shown during filling (diastole), for the (a) right ventricle, (b) left ventricle, and (c) single right ventricle. Axis units are in centimeters; the tissue boundary is colored in red and the inlet and outlet in purple; the inlet valve is partly open. Arrows report the individual anatomical coordinates z (longitudinal, directed from apex to base), x (from inlet to outlet), y (transversal).

contraction, or *systole*) or when it allows a gentle reception of the filling flow (during expansion, or *diastole*) without the need of high thrusts.

The fluid dynamics inside the three types of ventricles is reproduced for the population-average geometries of the RV, LV, and SRV under the assumption of a Newtonian fluid (with a kinematic viscosity of 0.04 cm^2/s). Numerical simulation is performed by an immersed boundary method inside a moving prescribed geometry, while the inlet valvular leaflets are moved by the flow and the outlet valve has a simple open-close behavior. Details of the numerical method were described in detail elsewhere and widely employed in previous studies [16,17].

Beside the flow pattern, the dynamic interactions between the flow and boundary are the principal focus for detecting the interplay between ventricular function and structural adaptation. It is important to recall that such interactions can only occur through an exchange of forces. In integral terms, the global force acting on a volume $V(t)$ of fluid (net of the inflating effect of the average pressure) is given by the gradient of the pressure field, $p(\mathbf{x}, t)$, where $\mathbf{x}$ is the 3D space coordinate and t is time, integrated on that volume, plus the viscous forces, $\tau(\mathbf{x}, t)$ integrated over the volume boundary $S(t)$:

$$\mathbf{F}(t) = \int_S \tau dS - \int_V \nabla p dV. \tag{1}$$

Force (1) can be rewritten in terms of the fluid velocity vector field, $\mathbf{v}(\mathbf{x}, t)$, by using the law of conservation of momentum (e.g., the Navier-Stokes equation):

$$\mathbf{F}(t) = \rho \int_V \left(\frac{\partial \mathbf{v}}{\partial t} + \mathbf{v} \cdot \nabla \mathbf{v} \right) dV. \tag{2}$$

Here ρ is the fluid density, which can be computed from the results of the fluid dynamic simulation.

In the case of an incompressible fluid, when the velocity vector field has zero divergence, the volume integral (2) can be transformed to a surface integral, accounting for the momentum exchanged at the solid boundary and across the open valvular orifices [18]:

$$\mathbf{F}(t) = \rho \int_S \left[\mathbf{x} \left(\frac{\partial \mathbf{v}}{\partial t} \cdot \mathbf{n} \right) + \mathbf{v}(\mathbf{v} \cdot \mathbf{n}) \right] dS. \tag{3}$$

This expression is simpler to compute as it allows evaluating the global hemodynamic force without the need of accurate knowledge of the entire intraventricular velocity field. Using Eq. (3), the global force vector can be estimated with negligible computational effort from the known geometry of all 192 cases. A dimensionless force, $\mathbf{F}/\rho g V$, is then presented after normalization with density, gravity acceleration g, and volume.

B. Results

The overall fluid dynamics arrangement can be qualitatively perceived by the steady-streaming (or heartbeat-averaged) flow pattern, which is displayed in Fig. 2 in terms of streamlines. Fluid dynamics in the LV and RV was extensively described in the literature (see, e.g., Ref. [17]). Briefly, the jet that enters the RV creates some vorticity that remains confined to the region below the valve; afterwards, during the systolic ejection, flow stretches along the converging outflow tract with a nearly potential velocity field. Differently, the flow entering the compact LV geometry develops a rotary motion that occupies the entire chamber; this rotation efficiently redirects the fluid toward the outflow for the following ejection. Such a relatively regular LV flow pattern is allowed by its nearly ellipsoidal geometry with the presence of an approximate symmetry plane (the x-z plane) containing the inflow, outflow, and apex. The geometry of the SRV approaches that of the LV; however, it originates from the peculiar RV shape and gives rise to a sort of LV with broken symmetry. This results in a fluid dynamics that differs substantially from both the RV and LV. Fluid enters the wide SRV and develops vorticity over the entire chamber; however, symmetries are important for the efficiency of cardiac flow [19] and their

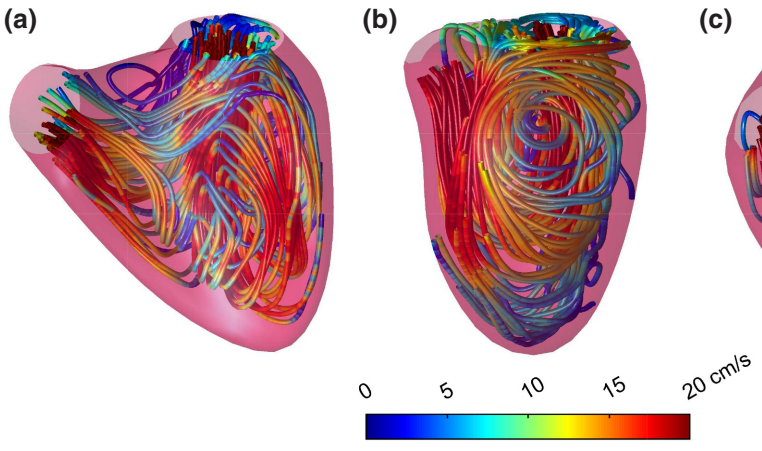

FIG. 2. Streamlines of the steady-streaming (heartbeat-average) flow for the (a) right ventricle, (b) left ventricle, and (c) single right ventricle. Streamlines are colored by velocity magnitude.

breaking does not allow creation of a regular circulation during filling and the following contraction develops in the presence of a velocity field that is weakly turbulent.

This qualitative picture of fluid flow can be employed as a reference for the interpretation of the global force exchanged between blood and the surrounding tissue. The three components of the dimensionless hemodynamic force vector (1) are shown in Fig. 3 that reports the average value of the value computed by Eq. (3) over the 64 individuals in each of the three groups. To ensure consistency, the time scale has been normalized to common end-systolic and end-diastolic instants before computing the average; the corresponding average volume curves are reported at the bottom for reference.

Consider first the forces that develop in the normal LV. During systolic ejection fluid is propelled toward the outflow tract along a direction that is mainly longitudinal (z axis), partly inclined along the inlet-outlet direction (x axis); during the diastolic filling the force acts mainly in the longitudinal direction with no net result in the other directions arising from the rotation. The transversal (y-axis) component is negligible all the time as a result of the approximate symmetry. These observations agree with and complete the picture previously reported in the clinical literature [20,21]. The analysis in the RV shows nearly comparable components along the three directions during systole according to the orientation of the RV outflow track along which fluid is propelled; differently, during diastole the filling is directed downward and the force is predominantly longitudinal, like in the LV.

The forces that develop in the SRV show a behavior that is by no means intermediate between the RV and LV. During both systole and diastole the force is predominantly longitudinal, indicating that the weak turbulence in blood motion does not produce any net coherent redirection, despite the lack of symmetry. More importantly, the overall magnitude of the force generated by the SRV is much lower, about one half that of either the RV or LV. This tells us about the reduced ability of the SRV to create and sustain blood flow: the geometric transformation from the RV to SRV is mainly a result of the need to support the higher systemic pressure, while it leads to a deterioration of the ventricular function. This deterioration of the SRV pumping function makes it potentially more prone to further structural adaptation.

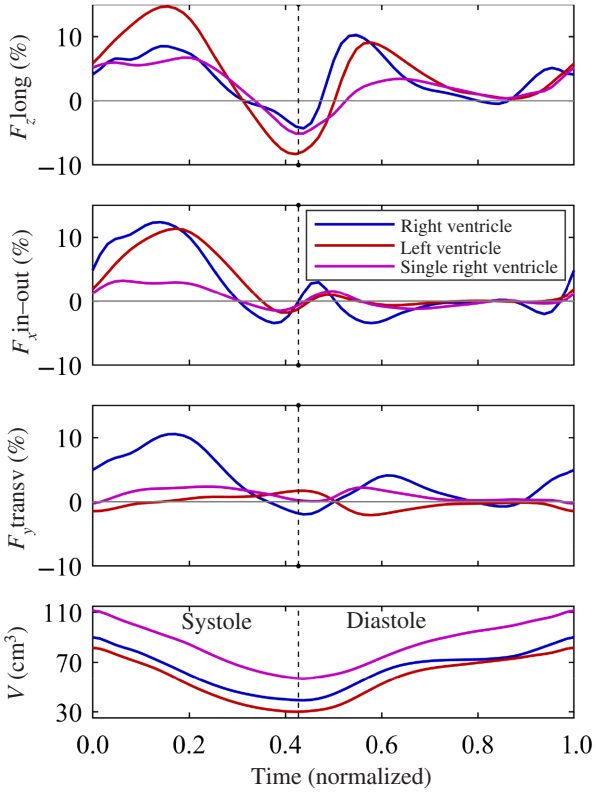

FIG. 3. Time course of the three components of the dimensionless hemodynamic force vector. Each curve represents the average computed from the 64 cases of each group. The volume curve is reported at the bottom, for timing reference.

IV. TISSUE DYNAMICS

A. Methods and theory

The dynamic properties of the cardiac tissue can be explored, noninvasively, by studying how deformations develop over time. They are described mathematically by the machinery of finite deformation [22]. Consider an initial state, say at a reference time $t = 0$ that is commonly taken at end diastole, where material points in the tissue are described by their coordinates $\mathbf{X}$, and a deformed state, say at a second time t, typically at end systole, where each material point has moved to a new position $\mathbf{x}(\mathbf{X}, t)$, such that $\mathbf{x}(\mathbf{X}, 0) = \mathbf{X}$. The transformation from $\mathbf{X}$ to $\mathbf{x}$ is described by the deformation gradient $\boldsymbol{\mathcal{F}}$ defined as

$$\mathcal{F}_{ij} = \frac{\partial \mathbf{x}_i}{\partial \mathbf{X}_j}. \tag{4}$$

Tensor $\boldsymbol{\mathcal{F}}$ can be separated through the polar decomposition in rotation and deformation

$$\boldsymbol{\mathcal{F}} = \boldsymbol{\mathcal{R}}\boldsymbol{\mathcal{U}}, \tag{5}$$

where $\boldsymbol{\mathcal{R}}$ is the rotation matrix, and $\boldsymbol{\mathcal{U}}$ is the right stretch tensor that contains information about the stretching that occurred during the time interval $(0, t)$. Along this approach, the straightforward definition for a strain tensor is

$$\boldsymbol{\mathcal{S}t} = \boldsymbol{\mathcal{U}} - \boldsymbol{\mathcal{I}} \tag{6}$$

with $\boldsymbol{\mathcal{I}}$ the identity matrix, which is known as the Lagrangian strain because it is computed following the

material points identified in the original configuration. It is also known as both the *Biot* strain tensor or engineering strain, because this definition corresponds to that used in the small-strain setting. Definition (6) represents the most intuitive description of the strain measure. For example, in 1D deformation, a segment of length L_0 is stretched (compressed) to a deformed length $L_1 = L_0 + \Delta L$ and the strain measures the relative change of length $\mathcal{S}t = \Delta L/L_0 = \lambda - 1$, where λ is the stretch, which is a measure of the effective elongation (shortening) of an originally undeformed fiber. This definition of strain is considered standard in clinical cardiology [23]. This study employs the Lagrangian strain (6) as a strain measure in the three-dimensional framework of the heart.

For the sake of completeness, it is worth recalling that several other definitions of strain based on the knowledge of $\boldsymbol{\mathcal{F}}$ are present in the literature. A common one is the *Green-Lagrange* strain tensor

$$\boldsymbol{\mathcal{S}t_G} = \tfrac{1}{2}(\boldsymbol{\mathcal{F}}^T\boldsymbol{\mathcal{F}} - \boldsymbol{\mathcal{I}}) = \tfrac{1}{2}(\boldsymbol{\mathcal{U}}^2 - \boldsymbol{\mathcal{I}}), \tag{7}$$

which was sometimes employed in cardiology [24–26]. It has the advantage of being obtained directly from $\boldsymbol{\mathcal{F}}$, without requiring the explicit calculation of $\boldsymbol{\mathcal{U}}$, thus allowing easier analytical manipulations. In the abovementioned example of 1D deformation, the Green-Lagrange strain is $\mathcal{S}t_G = \frac{1}{2}(\lambda^2 - 1)$, which has the disadvantage that the quadratic behavior does not correspond to the intuitive definition of physical deformation. Another popular definition is the *Hencky* strain tensor. In the previously mentioned 1D case, the Hencky strain has the remarkable property that it can be calculated as the time integral of the instantaneous strain rate dL/L, $\mathcal{S}t_H = \ln(L_1/L_0) = \int_0^1 dL/L$, for which it took the attribute of *natural* or *true* strain. Nevertheless, such a property is not valid in general and only applies in the case of axial deformations, in the absence of shear [27]. Therefore, all common strain definitions cannot be expressed as the time integral of a deformation rate associated with the symmetric part of the velocity gradient [28] and this approach is generally uncommon in solid mechanics since it requires the knowledge of a time-resolved course of deformation and does not allow us to express strain from the comparison of two configurations. Yet, it is important to remark that all the different strain tensor definitions (as well as the stretches, i.e., $\boldsymbol{\mathcal{U}}$ and $\boldsymbol{\mathcal{U}}^2$) share the same eigenvectors and the eigenvalues are directly related one to the other, thus allowing relative interchangeability among definitions.

The 2×2 strain tensor (6) is here evaluated on every element of the triangulated ventricular surface. To this end, consider a triangle of tissue identified during time by the coordinates of three material points $\mathbf{x}_i(t)$, with the index $i = 1, 2, 3$ spanning the three vertices. The three vertices of the triangular element identify a planar surface, with normal $\mathbf{n}$ defined by

$$\mathbf{n} = \frac{(\mathbf{x}_2 - \mathbf{x}_1) \times (\mathbf{x}_3 - \mathbf{x}_1)}{\|(\mathbf{x}_2 - \mathbf{x}_1) \times (\mathbf{x}_3 - \mathbf{x}_1)\|}. \tag{8}$$

A set of local material coordinates can be placed with the origin in the first vertex, the first axis directed to the second vertex, and another axis orthogonal to it and to normal (8). The set of unit coordinate vectors is then given by

$$\boldsymbol{\xi} = \frac{\mathbf{x}_2 - \mathbf{x}_1}{\|\mathbf{x}_2 - \mathbf{x}_1\|}, \qquad \boldsymbol{\eta} = \frac{(\mathbf{x}_2 - \mathbf{x}_1) \times \mathbf{n}}{\|(\mathbf{x}_2 - \mathbf{x}_1) \times \mathbf{n}\|}. \tag{9}$$

Unit vectors (8)–(9) provide a local orthonormal system of coordinates that translates and rotates with time. The deformation can be obtained from the description of the three vertices in the local coordinates $\mathbf{x}_i = [\xi_i, \eta_i, 0]$. This gives the simple expressions

$$\mathbf{x}_1 = [0, 0, 0], \tag{10a}$$

$$\mathbf{x}_2 = [\|\mathbf{x}_2 - \mathbf{x}_1\|, 0, 0], \tag{10b}$$

$$\mathbf{x}_3 = [(\mathbf{x}_3 - \mathbf{x}_1) \cdot \boldsymbol{\xi}, (\mathbf{x}_3 - \mathbf{x}_1) \cdot \boldsymbol{\eta}, 0]; \tag{10c}$$

because the three vertices lay on a plane, $\mathbf{x}_1$ is the origin and the first direction is aligned with $\mathbf{x}_2 - \mathbf{x}_1$. The resulting deformation gradient is

$$\boldsymbol{\mathcal{F}}(t) = \begin{bmatrix} \xi_2(t)/\xi_2(0) & [\xi_3(t) - \xi_2(t)\xi_3(0)/\xi_2(0)]/\eta_3(0) \\ 0 & \eta_3(t)/\eta_3(0) \end{bmatrix}, \tag{11}$$

from which it is immediate to extract the symmetric tensor $\boldsymbol{\mathcal{U}}^2 = \boldsymbol{\mathcal{F}}^T\boldsymbol{\mathcal{F}}$. Then the eigenvectors of $\boldsymbol{\mathcal{U}}^2$ are those of the strain tensor (6) and the corresponding eigenvalues are the square of the two principal stretches λ_i, $i = 1, 2$, from which the two principal strain values are $\mathcal{S}t_i = \lambda_i - 1$.

B. Results

Tissue contraction develops during systole: it starts from a reference undeformed configuration taken at end diastole, the instant when volume is maximum, and terminates at end systole, when volume is minimum and both strain eigenvalues are negative. The spatial distribution of the first principal strain [PS; the most negative eigenvalue of the strain tensor (6)] is shown in Fig. 4 averaged for the three groups; the color map is drawn over *strain lines* everywhere tangent to the corresponding eigenvector.

The value of the PS is comparable in the three ventricles, with slightly larger values in the LV, indicating that all produce a normal volumetric reduction. Differently, the strain-line patterns are qualitatively distinct. In the RV, the principal direction of contraction wraps around the valves and becomes more longitudinal toward the apex; this

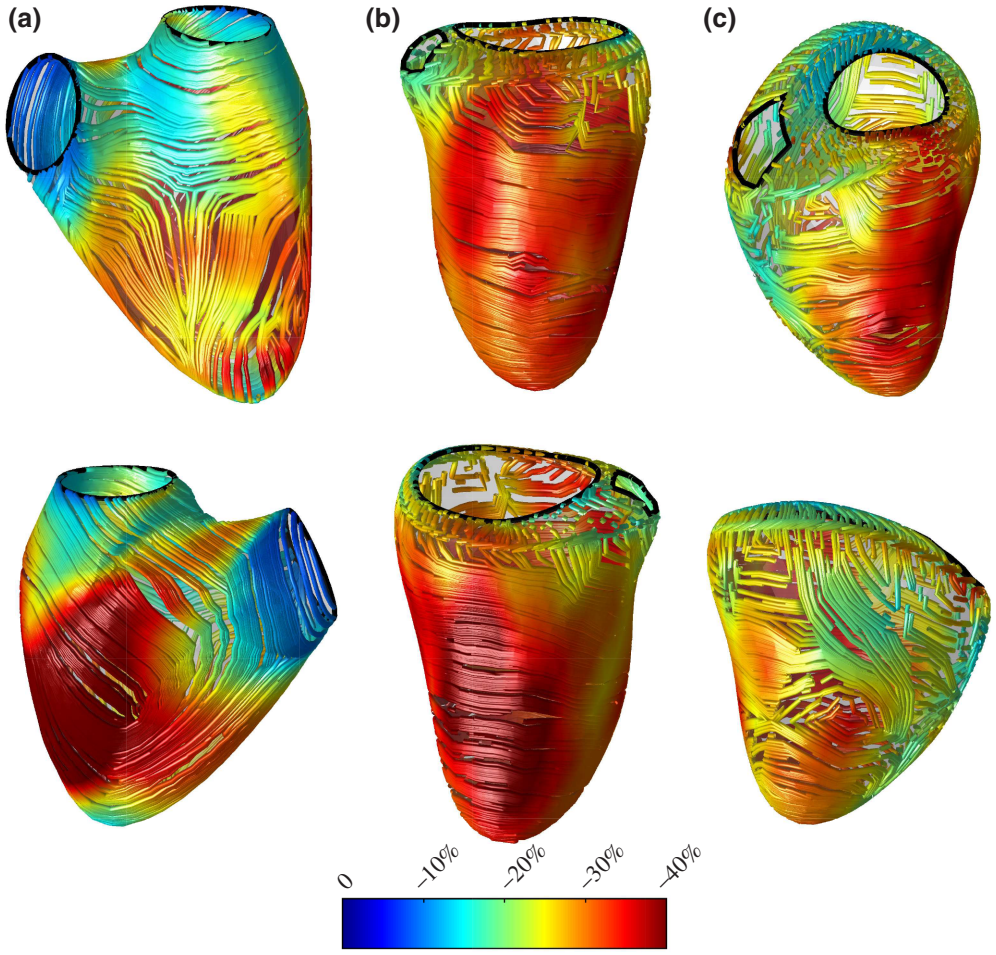

FIG. 4. Color map of the first principal strain (most-negative eigenvalue of the strain tensor) at the end of systolic contraction. Colors are drawn over the strain lines (tangent to the corresponding eigenvector) for the (a) right ventricle, (b) left ventricle, and (c) single right ventricle, with each shown in two opposite facing views.

directional pattern matches the arrangement of fibers in the surrounding muscular layer. The LV muscle is known to have a larger thickness with multiple layers where fibers are arranged in counter-rotating helices [29,30]; the contraction pattern observed here is dominantly circumferential, which is the result of a synergistic activation of layers containing fibers with cross-orientation, as previously observed in professional athletes [31]. Surprisingly, the pattern in the SRV is more similar to the LV; it presents a dominance of circumferential lines and does not correspond to what would result from the contraction of an inflated RV geometry (other than locally somewhere); this suggests that the SRV has built up a thickness with varying structure from that of the original RV.

A quantitative comparison of the global ventricular deformation is performed by reporting the time courses of the mean value of the PS and of the *secondary strain* (SS), defined as the second (less negative) eigenvalue of the strain tensor (6). As the PS represents the entity of contraction in the direction of strain lines displayed in Fig. 4, the SS acts in the direction perpendicular to them. The time profiles of the two global strains, averaged for each of the three groups, are reported in Fig. 5. The PS presents a similar behavior in the three ventricles with a slightly higher value in the LV, as noted before; this confirms that contraction is comparable because all ventricles ensure the normal volumetric pumping. However, the secondary strain curves differ significantly. The very low secondary strain value in the RV reflects the fact that the RV muscle is surrounded by a thin muscular layer with no room for fibers of varying orientation; therefore, muscle contraction develops along the principal direction, measured by the PS, and the absence of transverse fibers does not allow the development of a significant SS. The opposite occurs in the LV; here the circumferential principal direction does not correspond to the direction of fibers and is rather the result of the simultaneous contraction of multiple layers of counter-rotating helical fibers, which gives both the large PS and a significant SS that is about one half of the PS. The SRV presents an intermediate behavior, with a secondary strain about one third of the principal one: this observation requires the presence of a certain degree of multidirectional fibers and does allow considering the SRV as a RV with a changed, inflated geometry. It indicates that the SRV developed an adaptation that includes the growth in thickness with creation of new fibers, or reorientation of some existing ones, over novel directions with respect to those of the original RV.

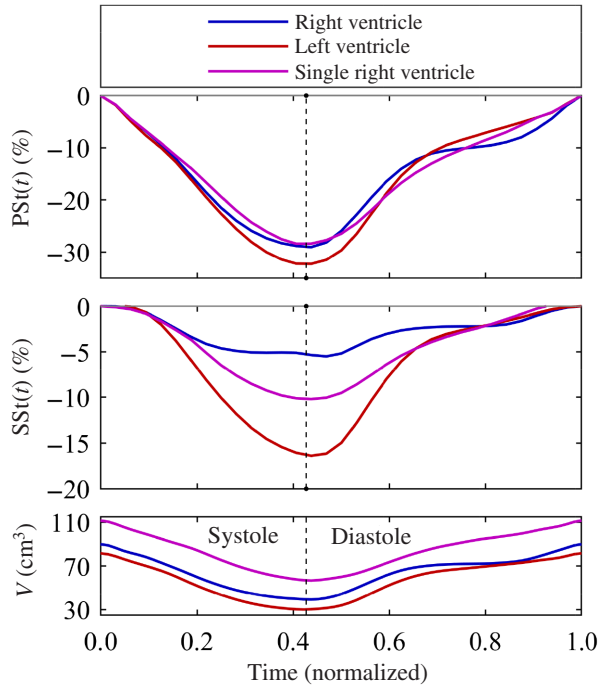

FIG. 5. Time courses of the first principal strain (PS) and of the secondary strain (SS). Each curve represents the average computed from the 64 cases of each group. The volume curve is reported at the bottom, for timing reference.

V. CONCLUSIVE DISCUSSION

Externally induced modifications to a biological system cause immediate functional alterations that are followed by a structural adaptive response in the longer term.

In the present case, the transformation from the RV to SRV rapidly produces soon after the Fontan operation (in the short term) a change of geometry induced by the higher systemic pressure. The new geometric configuration, however, involves a functional decrease of the associated fluid dynamics function with the reduction of the intraventricular pressure gradients, despite the fact that the volumetric pumping is preserved. This reduction implies the need to improve the force of contraction, which induces a progressive adaptive response of the surrounding muscular structure through an increase of thickness. However, it would take several months or years from the operation (long term) for the ventricle to adapt to the new condition by changing its original myocardial fibers. The present results indicate that such a thickening is not just a multiplication of the original fibers (like in hypertrophy), but rather a more efficient development of layers with variable directional arrangement, making the SRV work more closely to a LV; nevertheless, the original differences and symmetry break do not allow, in general, comparable performances to be reached. In this sense, this study provides initial evidence of an underlying poor mechanical performance, making the SRV at higher risk of adverse remodeling. Considering this insufficient adaptation of the SRV, it would be reasonable to expect progressive ventricular dysfunction over an even longer period.

In other words, a geometric change to a system delegated to a fluid dynamic function inevitably modifies its operational behavior in the short term. This alters the balance of forces exchanged between the fluid and the surrounding structure and may induce, in the longer term, a more profound structural adaptation. Revealing such a process requires a combined analysis of fluid dynamics and of structural response. Through this method, and supported by clinical data, the present analysis provides original information about the path followed after the transformation of the RV into a systemic SRV.

On average, the SRVs that deliver a normal function exhibit a structural adaptation that resembles a LV, although up to a limited degree. This incomplete adaptation is commonly accompanied by a small increase of SRV volume that goes with a small decrease of the SRV function, in terms of ejection fraction and strain. Larger volumes and reduced function are often used as prognostic values for the risk of adverse remodeling [32]. Nevertheless, the present results provide initial evidence that even such small changes can be associated with a large reduction in terms of fluid dynamic performance and a lower structural consistency; these effects may be considered when developing more sensible prognostic functional markers in conjunction with clinical indicators [33]. This makes the SRV at higher risk than normal ventricles and suggests more frequent monitoring of intimate functional properties to anticipate the development of progressive dysfunctional changes.

The interplay between fluid dynamics and structural changes is a general mechanism that can be extremely varied in the different fields of application. Uncovering the relative influences requires a combined evaluation of geometry, flow, and changes in the dynamics of the surrounding boundaries, taking into account the different time scales of the adaptation processes. Such an interplay is relevant in the presence of biological tissues and in cardiovascular mechanics, in particular, where the phenomenon of remodeling represents the driving macroscopic factor during the development of heart failure. In this respect, this study provides further support to the hypothesis that an alteration of fluid dynamics can represent the ignition cause for the cardiac adaptation of the surrounding solid structures.

In a more general perspective, this investigative study demonstrates, at least in the heart function, how application of a comprehensive mechanistic analysis allows uncovering underlying unstable conditions and anticipates the development of progressive structural adaptations.

ACKNOWLEDGMENT

D.C., L.Z. and G.P. acknowledge partial support by the Italian Ministry of Education, University and Research, under project PRIN 2017A889FP_006.

[1] G. Seminara, Fluvial sedimentary patterns, Ann. Rev. Fluid Mech. **42**, 43 (2010).

[2] J. Martins, Aerodynamic design optimization: Challenges and perspectives, Comput. Fluids **239**, 105391 (2022).

[3] J. R. Hove, R. W. Köster, A. S. Forouhar, G. Acevedo-Bolton, S. E. Fraser, and M. Gharib, Intracardiac fluid forces are an essential epigenetic factor for embryonic cardiogenesis, Nature **421**, 172 (2003).

[4] M. Midgett and S. Rugonyi, Congenital heart malformations induced by hemodynamic altering surgical interventions, Front. Physiol. **5**, 1 (2014).

[5] L. Andrés-Delgado and N. Mercader, Interplay between cardiac function and heart development, Biochim. Biophys. Acta – Mol. Cell. Res. **1863**, 1707 (2016).

[6] G. Pedrizzetti, G. L. Canna, O. Alfieri, and G. Tonti, The vortex – an early predictor of cardiovascular outcome? Nat. Rev. Cardiol. **11**, 545 (2014).

[7] Y. Nguyen, M. Ismail, F. Kabinejadian, E. Tay, and H. Leo, Post-operative ventricular flow dynamics following atrioventricular valve surgical and device therapies: A review, Med. Eng. Phys. **54**, 1 (2018).

[8] G. Pedrizzetti, A. R. Martiniello, V. Bianchi, A. D'Onofrio, P. Caso, and G. Tonti, Cardiac fluid dynamics anticipates heart adaptation, J. Biomech. **48**, 388 (2015).

[9] P. Sjöberg, J. Töger, E. Hedström, P. Arvidsson, E. Heiberg, H. Arheden, R. Gustafsson, S. Nozohoor, and M. Carlsson, Altered biventricular hemodynamic forces in patients with repaired tetralogy of fallot and right ventricular volume overload due to pulmonary regurgitation, Am. J. Physiol. – Circ. Physiol. **315**, H1691 (2018).

[10] A. Atz, V. Zak, L. Mahony, K. Uzark, N. D'agincourt, D. Goldberg, R. Williams, R. Breitbart, S. Colan, K. Burns, R. Margossian, H. Henderson, R. Korsin, B. Marino, K. Daniels, and B. McCrindle, Longitudinal outcomes of patients with single ventricle after the Fontan procedure, J. Am. Coll. Cardiol. **69**, 2735 (2017).

[11] J. Cao, K. Phana, J. Ayer, D. Celermajer, and D. Winlaw, Long term survival of hypoplastic left heart syndrome infants: Meta-analysis comparing outcomes from the modified Blalock–Taussig shunt and the right ventricle to pulmonary artery shunt, Int. J. Cardiol. **254**, 107 (2018).

[12] K. Inai, R. Inuzuka, H. Ono, M. Nii, S. Ohtsuki, Y. Kurita, A. Takeda, K. Hirono, K. Takei, S. Yasukouchi, T. Yoshikawa, Y. Furutani, E. Shimada, T. Shinohara, T. Shinozaki, Y. Matsuyama, H. Senzaki, and T. Nakanishi, Predictors of long-term mortality among perioperative survivors of Fontan operation, Eur. Heart J. **43**, 2373 (2022).

[13] S. Kutty, R. H. Rathod, D. A. Danford, and D. S. Celermajer, Role of imaging in the evaluation of single ventricle with the Fontan palliation, Heart **102**, 174 (2016).

[14] S. Suntratonpipat, N. Khoo, T. Colen, M. Alhabdan, D. Troung, N. Zahari, S. Kutty, J. Smallhorn, and E. Tham, Impaired single right ventricular function compared to single left ventricles during the early stages of alliation: A longitudinal study, J. Am. Soc. Echocardiogr. **30**, 468 (2017).

[15] T. Sato, R. Calderon, B. Klas, G. Pedrizzetti, and A. Banerjee, Simultaneous volumetric and functional assessment of the single right ventricle after Fontan palliation, utilizing three-dimensional speckle tracking echocardiography, Circ. J. **84**, 235 (2020).

[16] D. Collia, M. Vukicevic, V. Meschini, L. Zovatto, and G. Pedrizzetti, Simplified mitral valve modeling for prospective clinical application of left ventricular fluid dynamics, J. Comput. Phys. **398**, 108895 (2019).

[17] D. Collia, L. Zovatto, G. Tonti, and G. Pedrizzetti, Comparative analysis of right ventricle fluid dynamics, Front. Bioeng. Biotech. **9**, 667408 (2021).

[18] G. Pedrizzetti, On the computation of hemodynamic forces in the heart chambers, J. Biomech. **95**, 109323 (2019).

[19] G. Pedrizzetti and F. Domenichini, Nature Optimizes the Swirling Flow in the Human Left Ventricle, Phys. Rev. Lett. **95**, 108101 (2005).

[20] F. Vallelonga, L. Airale, G. Tonti, E. Argulian, A. Milan, J. Narula, and G. Pedrizzetti, Introduction to hemodynamic forces analysis: Moving into the new frontier of cardiac deformation analysis, J. Am. Heart Assoc. **10**, e023417 (2013).

[21] P. Arvidsson, J. Töger, M. Carlsson, K. Steding-Ehrenborg, G. Pedrizzetti, E. Heiberg, and H. Arheden, Left and right ventricular hemodynamic forces in healthy volunteers and elite athletes assessed with 4D flow magnetic resonance imaging, Am. J. Physiol. Heart Circ. Physiol. **312**, H314 (2016).

[22] R. Ogden, *Non-Linear Elastic Deformations* (Dover, New York, 1997).

[23] J. Voigt, G. Pedrizzetti, P. Lysyansky, T. Marwick, H. Houle, R. Baumann, S. Pedri, Y. Ito, Y. Abe, S. Metz, J. Song, J. Hamilton, P. Sengupta, T. Kolias, J. d'Hooge, G. Aurigemma, J. Thomas, and L. Badano, Definitions for a common standard for 2D speckle tracking echocardiography: Consensus document of the EACVI/ASE/industry task force to standardize deformation imaging, Eur. Heart J., Cardiovasc. Imag. **16**, 1 (2015).

[24] A. Satriano, B. Heydari, M. Narous, D. Exner, Y. Mikami, M. Attwood, J. Tyberg, C. Lydell, A. Howarth, N. Fine, and J. White, Clinical feasibility and validation of 3D principal strain analysis from cine MRI: Comparison to 2D strain by MRI and 3D speckle tracking echocardiography, Int. J. Cardiovasc. Imaging **33**, 1979 (2017).

[25] A. Evangelista, S. Gabriele, P. Nardinocchi, P. Piras, P. Puddu, L. Teresi, C. Torromeo, and V. Varano, A comparative analysis of the strain-line pattern in the human left ventricle: Experiments vs modelling, Comput. Methods Biomech. Biomed. Eng.: Imaging Visual. **4**, 164 (2016).

[26] A. Satriano, P. Pournazari, N. Hirani, D. Helmersen, M. Thakrar, J. Weatherald, J. White, and N. Fine, Characterization of right ventricular deformation in pulmonary arterial hypertension using three-dimensional principal strain analysis, J. Am. Soc. Echocardiogr. **32**, 385 (2018).

[27] A. Feeed, Hencky strain and logarithmic rates in Lagrangian analysis, Int. J. Eng. Sci. **81**, 135 (2014).

[28] G. Pedrizzetti, E. Kraigher-Krainer, A. DeLuca, G. Caracciolo, J. Mangual, A. Shah, L. Toncelli, F. Domenichini,

G. Tonti, G. Galanti, P. Sengupta, J. Narula, and S. Solomon, Functional Strain-Line Pattern in the Human Left Ventricle, Phys. Rev. Lett. **109**, 048103 (2012).

[29] G. Buckberg, J. Hoffman, A. Mahajan, S. Saleh, and C. Coghlan, Cardiac mechanics revisited: the relationship of cardiac architecture to ventricular function, Circulation **118**, 2571 (2008).

[30] G. Pedrizzetti, S. Sengupta, G. Caracciolo, C. Park, M. Amaki, G. Goliash, P. Sengupta, and J. Narula, Three-dimensional principal strain analysis for characterizing subclinical changes in left ventricular function, J. Am. Soc. Echocardiogr. **27**, 1041 (2014).

[31] L. Stefani, A. D. Luca, L. Toncelli, G. Pedrizzetti, and G. Galanti, 3D strain helps relating LV function to LV and structure in athletes, Cardiovasc. Ultrasound **2**, 33 (2014).

[32] M. Sobh, S. Freitag-Wolf, J. Scheewe, L. Kanngiesser, A. Uebing, D. Gabbert, and I. Voges, Serial right ventricular assessment in patients with hypoplastic left heart syndrome: A multiparametric cardiovascular magnetic resonance study, Eur. J. Cardiothorac. Surg. **61**, 36 (2022).

[33] D. Goldberg, C. Avitabile, M. McBride, and S. Parido, Exercise capacity in the Fontan circulation, Cardiol. Young **23**, 824 (2013).